Submitted to

International Europhysics Conference on High Energy Physics, July 12, 2001, Budapest

EPS 2001:	Abstract:	**798**
	Parallel Session	**1**
	Plenary Session	**Hard QCD, Structure Functions**

XX International Symposium on Lepton and Photon Interactions, July 23, 2001, Rome

LP 2001:	Abstract:	**491**
	Plenary Session	**S7,S8**

www-h1.desy.de/h1/www/publications/conf/conf_list.html

Measurement of Dijet Cross Sections in Photoproduction

H1 Collaboration

Abstract

Dijet cross sections as functions of various jet observables are measured in photoproduction using the H1 detector at HERA. The data sample comprises e^+p data collected from 1995-97. Jets are found using the inclusive $k_\perp$ algorithm with a minimum transverse momentum of the highest transverse momentum jet of 25 GeV. The results are compared to the predictions of next-to-leading order perturbative QCD.

1 Introduction

The production of high transverse momentum jets in γp-reactions is, to leading order, described by the pointlike interaction of real photons with the quarks (QCD compton effect) and the gluons (boson gluon fusion) of the proton. Higher order effects can be approximated by the notion of photonic parton densities which, analogously to proton parton densities, depend on a factorization scale μ_γ and x_γ, the longitudinal momentum fraction of the photon taken by the parton. The limiting case of pointlike interactions is thus given by $x_\gamma = 1$. At HERA these photoproduction reactions can be investigated in inelastic electron (positron) proton reactions at very small squared four-momentum transfers Q^2. Starting from the first investigation of this sort at HERA [1] the comparison of the results with the predictions of Quantum Chromo Dynamics (QCD) has been a central topic of interest [2].

High transverse momentum jets naturally provide a hard scale which makes perturbative QCD calculations reliable and renders the results less sensitive to non-perturbative physics. A measurement of jet cross sections at these high transverse momenta can therefore be used to test the current predictions of next-to-leading order (NLO) perturbative QCD – including the parameterizations of photon and proton parton densities at large scales – with high precision. The photonic quark densities have been extracted up to x_γ of 0.6 at scales up to $500\,\mathrm{GeV}^2$ investigating the photon structure function $F_{2,\gamma}$ in experiments at e^+e^--colliders[3]. This analysis extends the x_γ range up to 1 at scales between 600 and $6000\,\mathrm{GeV}^2$, where the quark density parameterizations of the photon are presently only partially constrained by measurements. The Photoproduction of jets is, in contrast to the $F_{2,\gamma}$-experiments directly sensitive to the gluon density of the photon, which by now is also only insufficiently known. Photoproduction data can be used to constrain the parton density functions in regions where only few measurements are available. In addition, the data is sensitive to the parton densities of the proton at x_P values up to 0.6. In this kinematical regime, the quark densities are well known from deep-inelastic scattering data, whilst the gluon density has uncertainties of the order 10 to 50 percent[4].

This paper is based on an e^+p-data sample collected with the H1 detector from 1995-1997 with an integrated luminosity of 34.9 pb $^{-1}$. It presents dijet cross sections in a range of observables for a sample of jet events with mean jet transverse energies $20 < E_T < 80\,\mathrm{GeV}$, observed x_γ values $0.1 < x_\gamma < 1$ and observed values of the fractional energies of the partons out of the proton $0.05 < x_P < 0.6$.

2 Jets in Photoproduction

2.1 Phenomenology

The cross section for the photoproduction of hard jets in electron-proton collisions can be calculated from the photon-proton scattering result using the well known factorization ansatz, where y is the longitudinal momentum fraction of the incoming photon and $f_{\gamma,e}$ is the Weizsäcker-Williams photon flux[5, 6, 7]:

$$\sigma_{eP\to eX} = \int dy f_{\gamma,e}(y)\sigma_{\gamma P}(y) \tag{1}$$

The hadronic photon-proton jet cross section can be calculated in perturbative QCD according to the factorization theorem. The cross section $\sigma_{\gamma P}$ is calculated as the convolution of the partonic cross sections with the parton momentum distributions of the proton $f_{i/P}$ and the photon $f_{j/\gamma}$. It is usually divided into a sum of two components, the pointlike part $\sigma_{\gamma P}^{\text{pointlike}}$, where the photon directly interacts with a parton out of the proton and the resolved part $\sigma_{\gamma P}^{\text{resolved}}$, where the photon first splits into partons which then interact with a parton out of the proton. This distinction is only unambiguously defined in leading order and depends on the photon factorization scale μ_γ. These components can be written as:

$$\sigma_{\gamma P}^{resolved} = \sum_{j,i} \int dx_\gamma f_{j/\gamma}(x_\gamma, \mu_\gamma) dx_P f_{i/P}(x_P, \mu_P) \hat{\sigma}_{ij}(\hat{s}, \mu_\gamma, \mu_P, \alpha_s(\mu_r), \mu_r) \quad (2)$$

$$\sigma_{\gamma P}^{pointlike} = \sum_{i} \int dx_P f_{i/P}(x_P, \mu_P) \hat{\sigma}_{i\gamma}(\hat{s}, \mu_\gamma, \mu_P, \alpha_s(\mu_r), \mu_r) \quad (3)$$

The squared center-of-mass energy of the hard subprocess is $\hat{s} = x_p x_\gamma y s$, where $\sqrt{s}$ is the total center of mass energy in the ep-system, i.e. 300 GeV at HERA. The proton factorization scale is μ_P, the renormalization scale is μ_r. The partonic cross sections $\hat{\sigma}$ can be expanded as a perturbative series in powers of α_s. These jet cross sections have been calculated up to the next-to-leading order in QCD[16, 18].

As can be seen from these equations the total cross section is obtained by integrating over y, x_p and x_γ. The partonic cross sections $\hat{\sigma}_{ij}$ and $\hat{\sigma}_{i\gamma}$ contain an integration e.g. over $\cos\theta^*$ the scattering angle in the center-of-mass system of the partonic two body reaction. In order to avoid mass singularities in the partonic cross section a minimum cut in θ^* or in the transverse energy of the outgoing partons has to be applied.

Much more detailed information on the reaction dynamics can be obtained by measuring differential cross sections in the kinematical observables. The two scaled longitudinal parton momenta x_γ and x_P can be calculated from the jets produced in the hard subprocess, using:

$$x_\gamma = \frac{1}{2E_e y}(E_{T,1}e^{-\eta_1} + E_{T,2}e^{-\eta_2}) \quad (4)$$

$$x_P = \frac{1}{2E_P}(E_{T,1}e^{\eta_1} + E_{T,2}e^{\eta_2}) \quad (5)$$

In this formula $E_{T,1}$ and $E_{T,2}$ are the transverse momenta of the two jets of the hard subprocess, η_1 and η_2 are their pseudorapidities and E_e and E_P are the energies of the electron and proton beams. The transverse momenta of the jets are equal for exclusive two jet production. The pseudorapidities of the jets give also access to θ^* via

$$\cos\theta^* = |\tanh((\eta_1 - \eta_2)/2)| \ . \quad (6)$$

Events at high y increase sensitivity to the low x_γ region, these at low y to high x_γ. Similarly, high E_T is correlated with high x_γ and x_P. These different kinematic regions in y and E_T are therefore sensitive to the photon and proton structure at different x_γ and x_P.

In principle one has to measure the dependence of the fourfold differential cross section on all four variables. This however requires a careful study of the resolution effects and a very large statistics. In this analysis therefore, more inclusive quantities like the distribution of the invariant mass of the two leading jets, M_{JJ}, and the transverse momentum distribution of the highest transverse momentum jet, $E_{T,max}$, are presented first. The cross section differential in the average value of the pseudorapidities $\overline{\eta} = (\eta_1 + \eta_2)/2$ is particularly sensitive to QCD calculations. It is thus presented for different photon-proton center-of-mass energies (y regions) and different scales ($E_{T,max}$ regions).

Single differential cross sections in x_γ and x_P, are measured in different scale regions (different $E_{T,max}$ regions) and for different x_γ or x_P cut-off values. The angle θ^* is sensitive to the kinematics of jet production and the differential cross section is therefore presented for different x_γ regions for all M_{JJ} and in addition with a cut-off in M_{JJ}. These angular distribution are also sensitive to the production of W or Z^0 bosons and would differ from QCD expectation if significant W or Z^0 production were occuring.

In this analysis, jets are always defined using the inclusive $k_\perp$ algorithm as proposed in [12, 13]. This works with a definition of jets in which not all particles are assigned to hard jets. The algorithm is applied in the laboratory frame and a separation parameter of 1 is used. An E_T weighted recombination scheme is used. The use of this algorithm has become standard in jet analyses at HERA [14].

2.2 QCD predictions and Models

To simulate the direct and resolved QCD photoproduction of jets, the PYTHIA 5.7 [8] and HERWIG 5.9 [9] event generators are used. Both programs contain the Born level QCD hard scattering matrix elements, regulated by a minimum cut-off. Leading logarithmic parton showers simulate higher order QCD radiation. GRV-LO [10] parton distribution functions (PDFs) for the proton and photon are used. The Lund String model is used by PYTHIA to hadronize the outgoing partons, while HERWIG uses the Cluster Hadronization approach. Multiple interactions between the proton and resolved photon are dealt with in PYTHIA by adding soft processes within the same event. These processes are calculated by extending the perturbative parton-parton scattering to a low E_T cut-off. In HERWIG (in order to model the multiple interactions), 35% of events were simulated to contain so called *soft underlying events*. In order to obtain a realistic description of the data a full detector simulation [11] is applied to all Monte Carlo events.

The measured cross sections are compared to perturbative QCD calculations. The LO and NLO dijet cross sections are calculated using a program based on the subtraction method [16, 17] for the analytic cancellation of infrared singularities. In calculating LO and NLO cross sections a 2-loop α_s is taken with 5 flavours. Λ_{QCD} is set to 0.226 GeV, which is the value used in the proton parton density functions. CTEQ5M[28] parton density functions were chosen for the proton. MRST99[29] parton density functions were used to test the dependence of the NLO cross sections on the proton PDF uncertainties. For the photon we have chosen GRV-HO[19] as a main setting and the parameterizations of GS-HO[21] and AFG-HO[20] for comparisons. The renormalization scale μ_r and the factorization scales, μ_p and μ_γ have been set to the sum of the transverse momenta of the outgoing partons divided by two. The QCD program allows the variation of this scale. It was varied from 0.5 to 2 times the default scale to estimate the scale uncertainty of the NLO calculation. This uncertainty is approximately ± 10 to 20%.

3 Experimental Technique

3.1 H1 Detector

The H1 detector is described in detail in [22]. Only those components relevant to the analysis are briefly described here. The Liquid Argon (LAC) [23] and SpaCal [24] calorimeters are used to trigger events, reconstruct the hadronic energy of the final state and anti-tag positrons. The central tracking detector (CTD) is used to reconstruct the interaction vertex and to supplement the measurement of hadronic energy flow. A coordinate system in which the nominal interaction point is at the origin and the incident proton beam defines the $+z$ direction is used.

The LAC covers the polar angle range $4° < \theta < 154°$ with full azimuthal acceptance. It consists of an electromagnetic section and a hadronic section. The total depth varies between 4.5 and 8 hadronic interaction lengths. The angular region $153° < \theta < 177.8°$ is covered by the SpaCal, a lead/scintillating-fibre calorimeter. It consists of an electromagnetic and a hadronic section.

The CTD consists of two concentric cylindrical drift chambers, coaxial with the beam-line, with a polar angle coverage of $15° < \theta < 165°$. The entire CTD is immersed in a 1.15 T magnetic field. The luminosity determination is based on measurement of the $ep \to ep\gamma$ Bethe-Heitler process, where the positron and photon are detected in crystal Cherenkov calorimeters located downstream of the interaction point.

3.2 Event Selection

The data sample was collected with the H1 detector from 1995-97, when 820 GeV protons collided with 27.6 GeV positrons, in HERA, resulting in a centre-of-mass energy of 300 GeV. The obtained integrated luminosity was 34.9 pb^{-1}. The events were triggered by a standard set of electromagnetic energy and missing energy triggers. The trigger efficiencies are above 94 percent for the event sample described in this analysis. Energy deposits in the calorimeters and tracks in the CTD were combined to reconstruct the hadronic energy of events [25]. It was required that an event vertex was reconstructed within 35 cm of the nominal z position.

A cut on the missing transverse momentum $E_{T,miss} <$ 20 GeV is imposed to remove Charged Current and non-ep events. A special cosmic finder is used to remove remaining cosmic events. The measured jet energies are calibrated to their true energies. The calibration of the jet energies is tested by the jet-electron balance with deep inelastic scattering events and the jet-jet balance for this photoproduction sample in different kinematic regions. The Monte Carlo description of the jet energy calibration was found to be better than 3 percent.

The most significant background in the data sample arises from neutral current deep-inelastic scattering events. Deep-inelastic scattering dijet data and the ARIADNE [26] Monte Carlo interfaced with DJANGO [27] are used to estimate these backgrounds, which are suppressed by removing events with an electron identified in the LAC or SpaCal and by requiring $y < 0.9$, with y reconstructed using hadronic variables [15]. Further electron finding algorithms reduce this background to less than 1% for the total sample. In the bins with the highest y at low $\overline{\eta}$ this background is estimated to be 5% at maximum and was subtracted on a statistical basis.

Asymmetric cuts on the E_T of the highest transverse momentum jets are needed in order to avoid NLO uncertainties due to infrared-sensitive regions of phase space [16]. The jet selection criteria require that the E_T of the highest transverse momentum jet $E_{T,max} > 25$ GeV, and the transverse momentum of the second highest transverse momentum jet $E_{T,second} > 15$ GeV. The pseudorapidity of each jet, η is restricted to $-0.5 < \eta_{Jet} < 2.5$. All jets are then well contained in the LAC. The measured kinematic region is restricted to $0.1 < y < 0.9$ and $Q^2 < 1$ GeV^2.

The total number of events found was then 4732.

3.3 Correction of the Data for Detector effects

The data are corrected for detector effects such as limited resolution and ineffiencies. To determine these effects the HERWIG and PYTHIA Monte Carlo samples are used. Both programs describe all tested jet distributions well. The bin sizes of all distributions are chosen to give an efficiency and purity above 30-50 percent. The correction is done by using the bin-to-bin method. This is possible due to the good detector resolution and the obtained bin purities. The mean values of the two Monte Carlo generators are taken for the correction. The correction functions of the two models are in good agreement and differ on average by 5 $\%$ and at most by 20 $\%$. All correction factors lie typically between 0.9 and 1.2 and reach in some cases 1.5.

3.4 Systematic Uncertainties

The following sources of systematic error were considered:

- An 4% uncertainty on the LAr energy scale which results in an uncertainty with a mean value of 20% on the jet cross sections.
- An 8% uncertainty of the hadronic Spacal energy scale which results in an uncertainty of 1 % for all bins in the jet cross sections.
- Half the difference between HERWIG and PYTHIA is taken as the uncertainty of the detector correction. The resulting uncertainty on the jet cross sections is in the range of 5 to 10%.
- The uncertainty in the trigger efficiency results in an error of $\sim 3\%$ on the cross section.
- The uncertainty on the background substraction results in an error on the cross sections of $\sim 2\%$.
- The uncertainty in the integrated luminosity results in an overall normalization error of 1.5% on the cross section.

All systematic errors are added in quadrature. The resulting systematic uncertainty ranges from 20 to 30 percent and is larger than the statistical uncertainty.

The effect of multiple scattering is tested by comparing the data to HERWIG with and without some fraction P of soft underlying events. If P is ~ 30 to 35% the jet-profiles are well described for all regions of x_γ. The difference of HERWIG for the obtained cross sections with and without 35 percent of soft underlying events is below 5-10 percent for x_γ between 0.3-0.8 and 10-20 percent for $x_\gamma < 0.3$. For $x_\gamma > 0.8$ the difference is negligible. Neither for these effects nor for the underlying event energies corrections are applied.

4 Results

The measured cross sections for inclusive dijet production in the reaction $e+p \to e+p+$jets are presented as single differential cross sections for all distributions. The data are always corrected for detector effects and presented for the phase space region defined in section 3.2. The inner error bars of the data points denote the statistical, the outer error bars the quadratic sum of all statistical and systematic uncertainties. All results are compared to next-to-leading order (NLO) QCD predictions. The NLO QCD prediction is always obtained with our standard setting (described in section 2) if not quoted. In addition the predictions of NLO QCD corrected for hadronization effects are shown. The hadronization effects are obtained with the PYTHIA and HERWIG Monte Carlos and the mean value of the two predictions is used for corrections. Here the difference between the two Monte Carlo models is generally very small and at maximum 10 percent in some bins of the measured cross sections.

In figure 1 the dijet cross section is shown as a function of the invariant mass M_{JJ} of the dijet system. The data is presented for M_{JJ} values between 45 and 180 GeV. The measured cross section falls by more than 3 orders of magnitude. Hadronization corrections are less than 5 percent for all bins. NLO QCD describes the measured data for the whole mass range, while the calculation using LO matrix elements fails to describe the low M_{JJ} region. This is partly due to the fact that the low M_{JJ} region is populated by events which are influenced by the asymmetric cuts on the jet transverse momenta. Events in which the second jet has an E_T less than 25 GeV contribute mainly in this region and are only present in dijet calculations beyond the leading order. These observations agree with the fact that the scale uncertainties of the QCD predictions are largest at low M_{JJ} values.

The dijet cross section as a function of the transverse momentum of the highest transverse momentum jet $E_{T,max}$ is shown in figure 2. The distribution demonstrates that the data is well described by NLO QCD up to the highest $E_{T,max}$ bin. The cross sections are little affected by hadronization corrections which are around 5 percent for all bins.

The differential cross section $d\sigma/d\overline{\eta}$ is displayed for two different y regions and two $E_{T,max}$ bins in figure 3. An overall agreement between data and NLO QCD is observed taking into account the uncertainties of the calculations and data points. At low $\overline{\eta}$, where direct interactions are dominant, the QCD predictions lie above the data, but hadronization corrections are largest in this region and these corrections lower the partonic predictions. Nevertheless the predictions tend to lie slightly above the data at low $\overline{\eta}$. At high $\overline{\eta}$, where resolved interactions are dominant and hadronization corrections are small, the NLO QCD predictions agree well with the measured data taking into account the experimental and theoretical uncertainties.

The upper plots in figure 4 show the dijet cross section $d\sigma/dx_\gamma$ as a function of x_γ for two different x_P regimes. The data lie below the calculations only for $x_\gamma > 0.85$. Again, hadronization corrections are largest in this region and reduce this discrepancy. Different proton PDF sets (MRST99 1-3,CTEQ5M) result in differences of less than 5 percent for the predicted cross section for $x_P < 0.1$ and up to 10 percent for $x_P > 0.1$. Therefore, the differences in the proton PDFs are less than the scale uncertainties for $x_P < 0.1$ and of the same order for $x_P > 0.1$. These findings are corroborated by the lower part of figure 4 where the cross section $d\sigma/dx_P$ as a function of x_P is shown for two different x_γ regions. Even at the highest x_P the measured cross section agrees well with the QCD predictions.

Figure 5 displays the dijet cross sections $d\sigma/dx_\gamma$ as a function of x_γ for two regions of $E_{T,max}$, representing different factorization scales for the photon and proton PDFs. The data is compared to NLO calculations with three different parameterizations of the photon structure. All these predictions are NLO QCD calculations corrected for hadronization effects. The predictions vary only little with the photon PDFs used. In contrast the NLO scale uncertainties produce a significant effect as can be inferred from figure 6. For high values of x_γ hadronization correction have a sizeable influence. Again for the direct dominated part at high x_γ the data is slightly below all predictions.

A more sensitive comparison between data and theory is obtained by plotting the relative difference as shown in figure 7. The symbol σ stands for $d\sigma/dx_\gamma$. In contrast to the other figures the error bars of the data only contain the uncorrelated systematic errors, the correlated errors due to the uncertainty of the calometric energy are shown as a hatched band. The figure clearly demonstrates that these uncertainties and the NLO scale uncertainties are much more important than the differences induced by using different photon PDFs. All NLO predictions shown in the figure include hadronization corrections.

Finally, the dijet cross section $d\sigma/d\cos\theta^*$ is plotted in figure 8 for $x_\gamma > 0.8$ and $x_\gamma < 0.8$ (upper two plots). Again, the data are well described by NLO QCD for low x_γ, whereas at higher x_γ the predictions overshoot the data for small values of $\cos\theta^*$. In addition these cross sections are shown with a cut on the invariant mass M_{JJ} of the dijet system (lower two plots). Although this cut changes the shape of the distribution dramatically, the QCD calculations reproduce this behavior nicely.

5 Conclusions

New measurements of dijet events in photoproduction at high transverse momentum are presented for various jet kinematic observables. The measurements cover invariant dijet masses up to $160\,\mathrm{GeV}$ and transverse momenta up to $75\,\mathrm{GeV}$. In this kinematic domain non-perturbative effects like multiple scattering and hadronization are found to be small, which allows a direct comparison to QCD calculations to be made. The results again demonstrate the power of perturbative QCD in predicting the measured cross sections in a wide kinematical range. Even though the photon PDFs have been obtained from measurements at lower scales, their QCD evolution correctly reproduces the data at high scales. A further improvement in testing the theory can only be reached by reducing the theoretical scale uncertainties and the systematic uncertainties of the data.

Acknowledgements

We are grateful to the HERA machine group whose outstanding efforts have made and continue to make this experiment possible. We thank the engineers and technicians for their work in constructing and now maintaining the H1 detector, our funding agencies for financial support, the DESY technical staff for continual assistance, and the DESY directorate for the hospitality which they extend to the non-DESY members of the collaboration. We wish to thank S. Frixione and B. Pötter for many helpful discussions.

References

[1] H1 Collab., T. Ahmed et al., Phys. Lett. **B 297** (1992) 205

[2] H1 Collab., C. Adloff et al., Phys. Lett. **B 483** (2000) 36;
H1 Collab., C. Adloff et al., Eur. Phys. J. **C 1** (1998) 97;
ZEUS Collab., J. Breitweg et al., Eur. Phys. J. **C 1** (1998) 109;
ZEUS Collab., J. Breitweg et al., Eur. Phys. J. **C 11** (1999) 35;

[3] R. Nisius, Phys. Reports **332** (2000) 165

[4] J. Huston et al, Phys. Rev. **D 58** (1998) 114034

[5] P. Kessler, Il Nuovo Cimento **17** (1960) 809

[6] V.M. Budnev et al., Phys. Rep. **C 15** (1974) 181

[7] S. Frixione et al., Phys. Lett. **B 319** (1993) 339

[8] T. Sjostrand, CERN-TH-6488 (1992), Comput. Phys. Commun. **82** (1994) 74.

[9] G. Marchesini et al., Comp. Phys. Comm. **67** (1992) 465.

[10] M. Glück, E. Reya and A. Vogt, Phys. Rev. **D46** (1992) 1973.

[11] R. Brun et al., GEANT3 User's Guide, CERN-DD/EE-84-1 (1987).

[12] S.D. Ellis and D.E. Soper, Phys. Rev. **D48** (1993) 3160

[13] S. Catani, Yu.L. Dokshitzer, M.H. Seymour and B.R. Webber , Nucl. Phys. **B 406** (1993) 187

[14] H1 Collab., C. Adloff et al., Eur. Phys. J. **C 19** (2001) 289

[15] A. Blondel and F. Jacquet, Proceedings of the Study of an ep Facility for Europe ed. U. Amaldi, DESY 79/48 (1979) 391.

[16] S. Frixione and G. Ridolfi, Nucl. Phys. **B507** (1997) 315

[17] S. Frixione, Nucl. Phys. **B 507** (1997) 295

[18] M. Klasen, G. Kramer, Z. Phys. **C 76** (1997) 67 ;
B.W. Harris, J.F. Owen, Phys. Rev. **D 56** (1997) 4007;
P. Aurenche et al., Eur. Phys. J. **C 17** (2000) 413;

[19] M. Glück, E. Reya and A. Vogt , Phys. Rev. **D45** (1992) 3986

[20] P. Aurenche, J.P. Guillet and M. Fontannaz, Z.Phys. **C64** (1994) 621

[21] L.E. Gordon, J.K. Storrow, Nucl.Phys. **B489** (1997) 405

[22] H1 Collaboration, I. Abt et al., Nucl. Instr. Meth. **A 386** (1997) 310 and 348

[23] H1 Calorimeter Group, B. Andrieu et al., Nucl. Instr. and Meth. **A336** (1993) 460.

[24] H1 SpaCal Group, R. D. Appuhn et al., Nucl. Instr. and Meth. **A386** (1997) 397.

[25] H1 Collab., C. Adloff et al., Z. Phys. **C74** (1997) 221.

[26] L. Lönnblad, Comp. Phys. Comm. 71 (1992) 15

[27] K. Charchula et al., Comp. Phys. Comm. 81 (1994) 381

[28] CTEQ Collaboration, H.L. Lai et al., Phys. Rev. **D55** , (1997), 1280

[29] A. D. Martin, R. G. Roberts, W. J. Stirling, R. S. Thorne, Eur. Phys. J. **C 14** (2000), 133

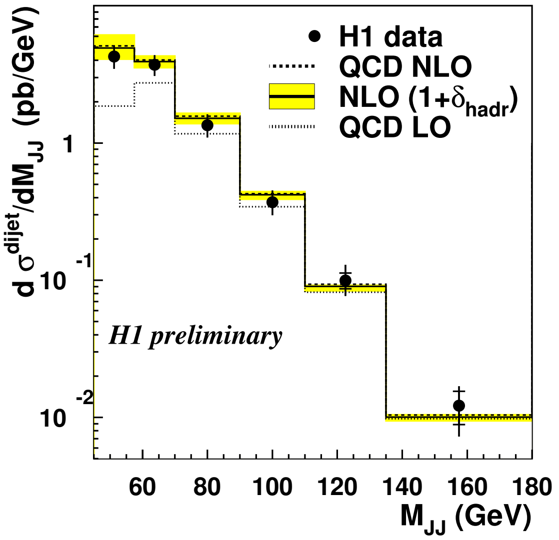

Figure 1: Differential eP cross sections for dijet production as a function of the invariant dijet mass M_{JJ} of the two highest E_T jets. The inner error bars denote the statistical, the outer error bars the quadratic sum of all statistical and systematic errors of the data. The LO predictions using CTEQ5M structure functions for the proton and GRV-HO structure functions for the photon are shown as a dotted line. NLO predictions with the same structure functions are shown as a dashed line. NLO predictions with hadronization corrections are shown as a full line, the grey band indicates the renormalization and factorization scale uncertainties of the NLO prediction.

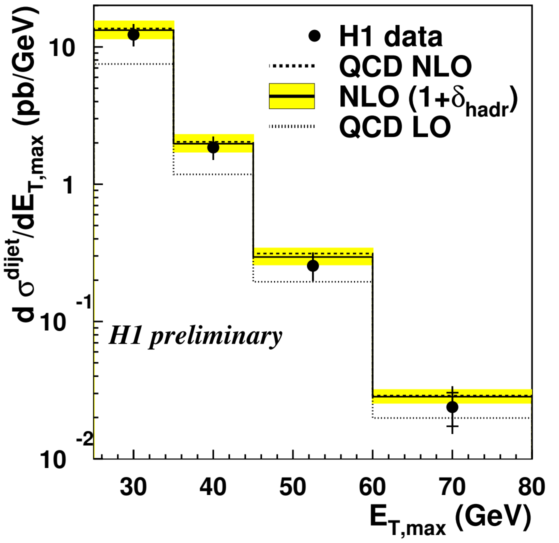

Figure 2: Differential eP cross sections for dijet production as a function of the E_T of the highest E_T jet $E_{T,max}$. The inner error bars denote the statistical, the outer error bars the quadratic sum of all statistical and systematic errors of the data. The LO predictions using CTEQ5M structure functions for the proton and GRV-HO structure functions for the photon are shown as a dotted line. NLO predictions with the same structure functions are shown as a dashed line. NLO predictions with hadronization corrections are shown as a full line, the grey band indicates the renormalization and factorization scale uncertainties of the NLO prediction.

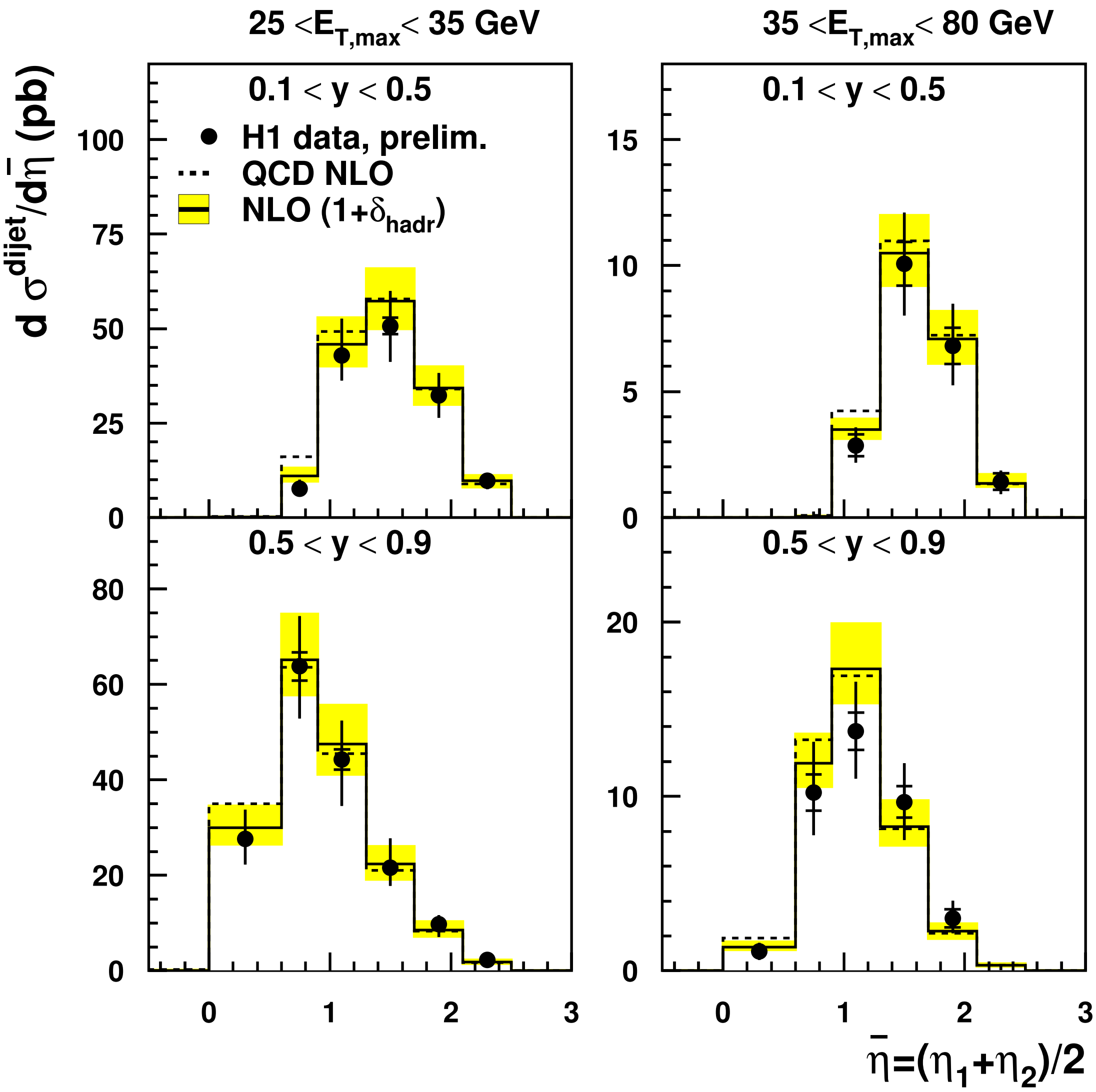

Figure 3: Differential eP cross sections for dijet production as a function of the $\overline{\eta}$ of the two highest E_T jets. The upper plots show the low y and the lower plots the high y region. The left plots show the low $E_{T,max}$ and the right plots the high $E_{T,max}$ region. The inner error bars denote the statistical, the outer error bars the quadratic sum of all statistical and systematic errors of the data. NLO predictions using CTEQ5M structure functions for the proton and GRV-HO structure functions for the photon are shown as a dashed line. NLO predictions with hadronization corrections are shown as a full line, the grey band indicates the renormalization and factorization scale uncertainties of the NLO prediction.

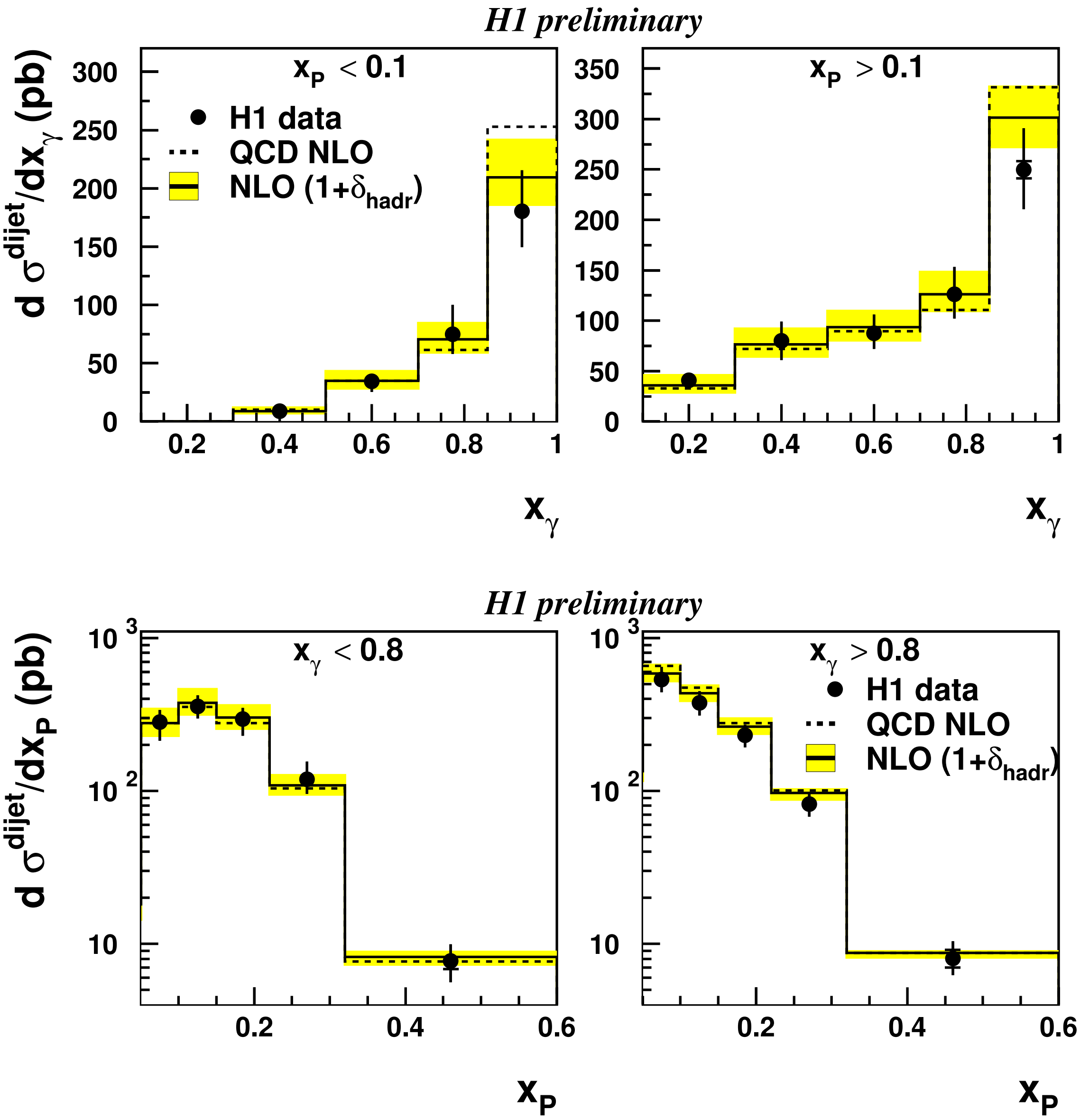

Figure 4: Differential eP cross sections for dijet production as a function of x_γ (upper plots) and x_P (lower plots). The upper left plot shows the cross sections as a function of x_γ for the lower x_P region, the upper right plot for the higher x_P region. The lower right plot shows the cross sections as a function of x_P for the higher x_γ region, the lower left plot for the lower x_γ region. The inner error bars denote the statistical, the outer error bars the quadratic sum of all statistical and systematic errors of the data. The NLO predictions using CTEQ5M structure functions for the proton and GRV-HO structure functions for the photon are shown as a dashed line. NLO predictions with hadronization corrections are shown as a full line, the grey band indicates the renormalization and factorization scale uncertainties of the NLO prediction.

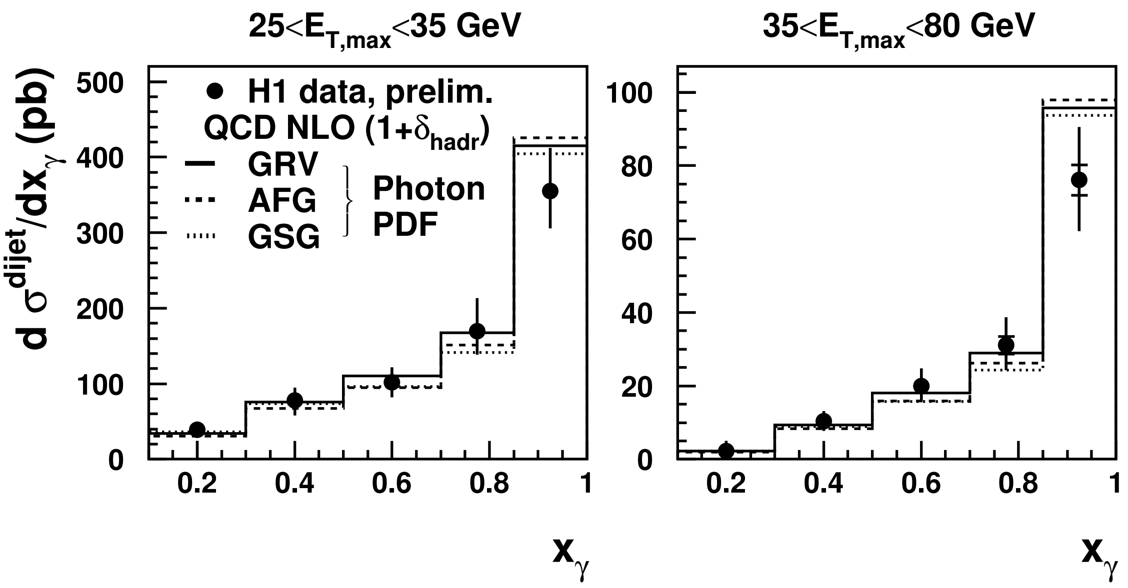

Figure 5: Differential eP cross sections for dijet production as a function of x_γ. The left plot shows the cross sections for the lower $E_{T,max}$ region, the right plot for the higher $E_{T,max}$ region. The inner error bars denote the statistical, the outer error bars the quadratic sum of all statistical and systematic errors of the data. The NLO predictions using CTEQ5M structure functions for the proton and GRV-HO structure functions for the photon and including hadronization corrections are shown as a full line. NLO predictions using AFG-HO and GSG-HO parametrizations of the photon structure functions and including hadronization corrections are shown as dashed (AFG) and dotted (GSG) line.

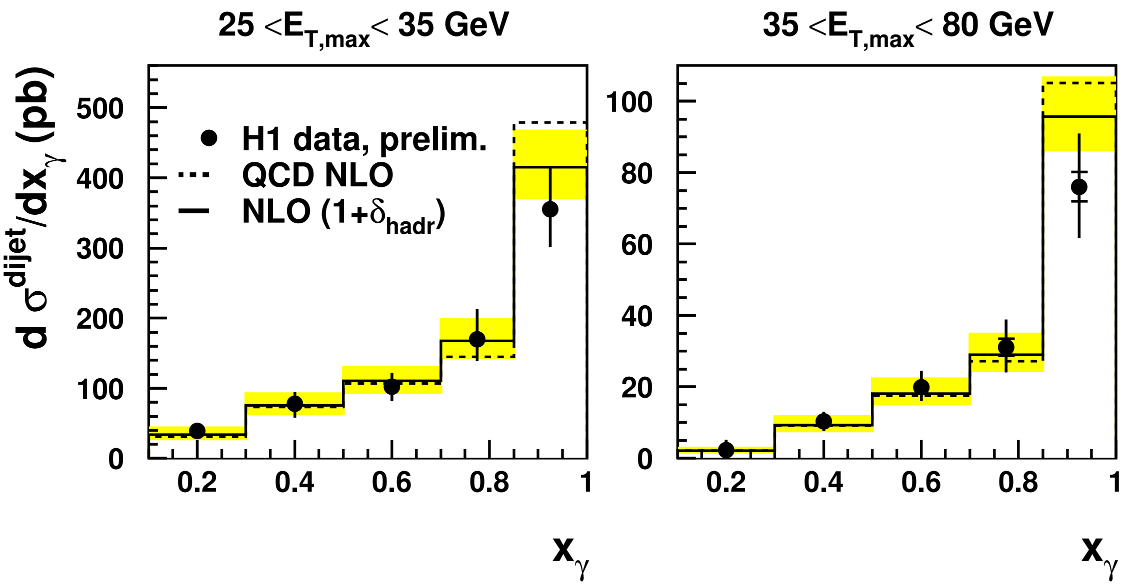

Figure 6: Differential eP cross sections for dijet production as a function of x_γ. The left plot shows the cross sections for the lower $E_{T,max}$ region, the right plot for the higher $E_{T,max}$ region. The inner error bars denote the statistical, the outer error bars the quadratic sum of all statistical and systematic errors of the data. The NLO predictions using CTEQ5M structure functions for the proton and GRV-HO structure functions for the photon are shown as a dashed line. NLO predictions with hadronization corrections are shown as a full line, the grey band indicates the renormalization and factorization scale uncertainties of the NLO prediction.

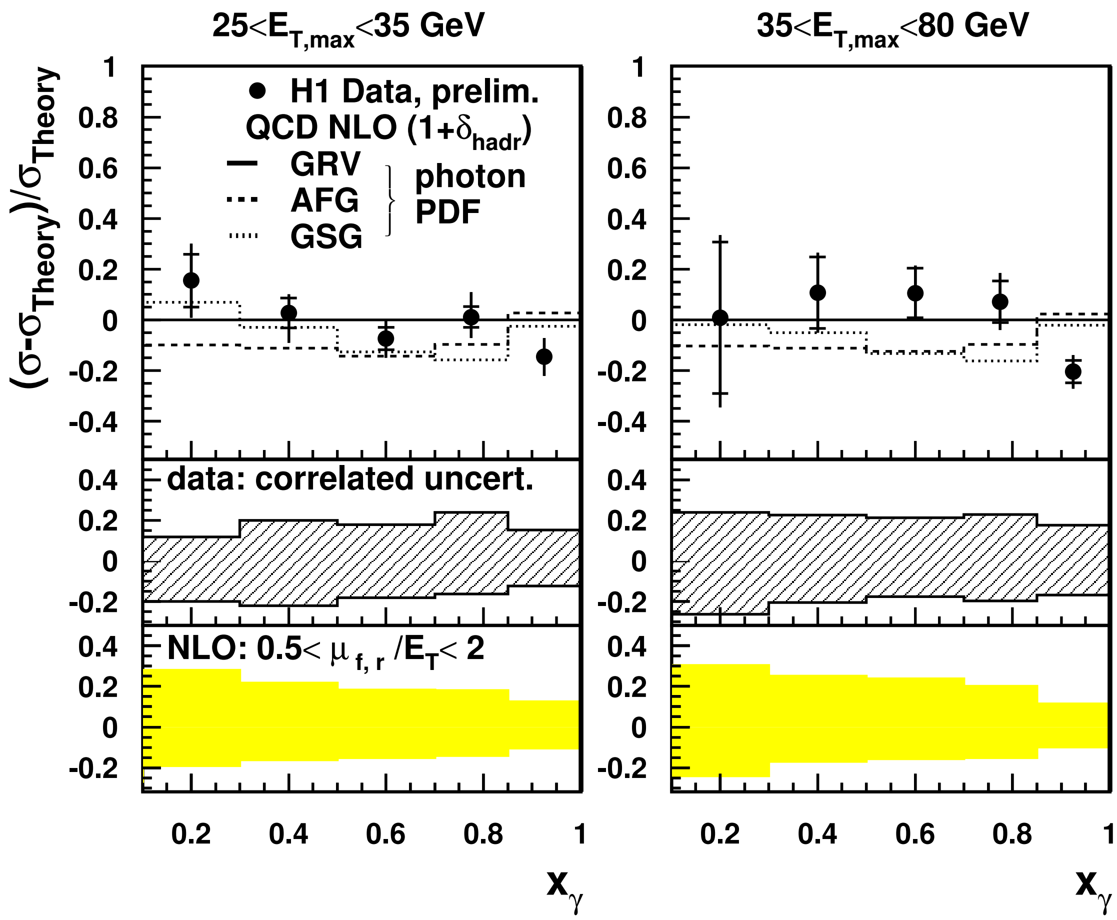

Figure 7: The relative difference of the dijet cross sections as a function of x_γ to the NLO prediction with hadronization corrections applied using CTEQ5M structure functions for the proton and GRV-HO structure functions for the photon. The data is shown as points. The inner error bars denote the statistical, the outer error bars the quadratic sum of all statistical and of the uncorrelated systematic errors of the data. The correlated systematic errors are shown in the middle two plots as a shaded band. The grey band (two lower plots) shows the renormalization and factorization scale uncertainties of this NLO prediction.

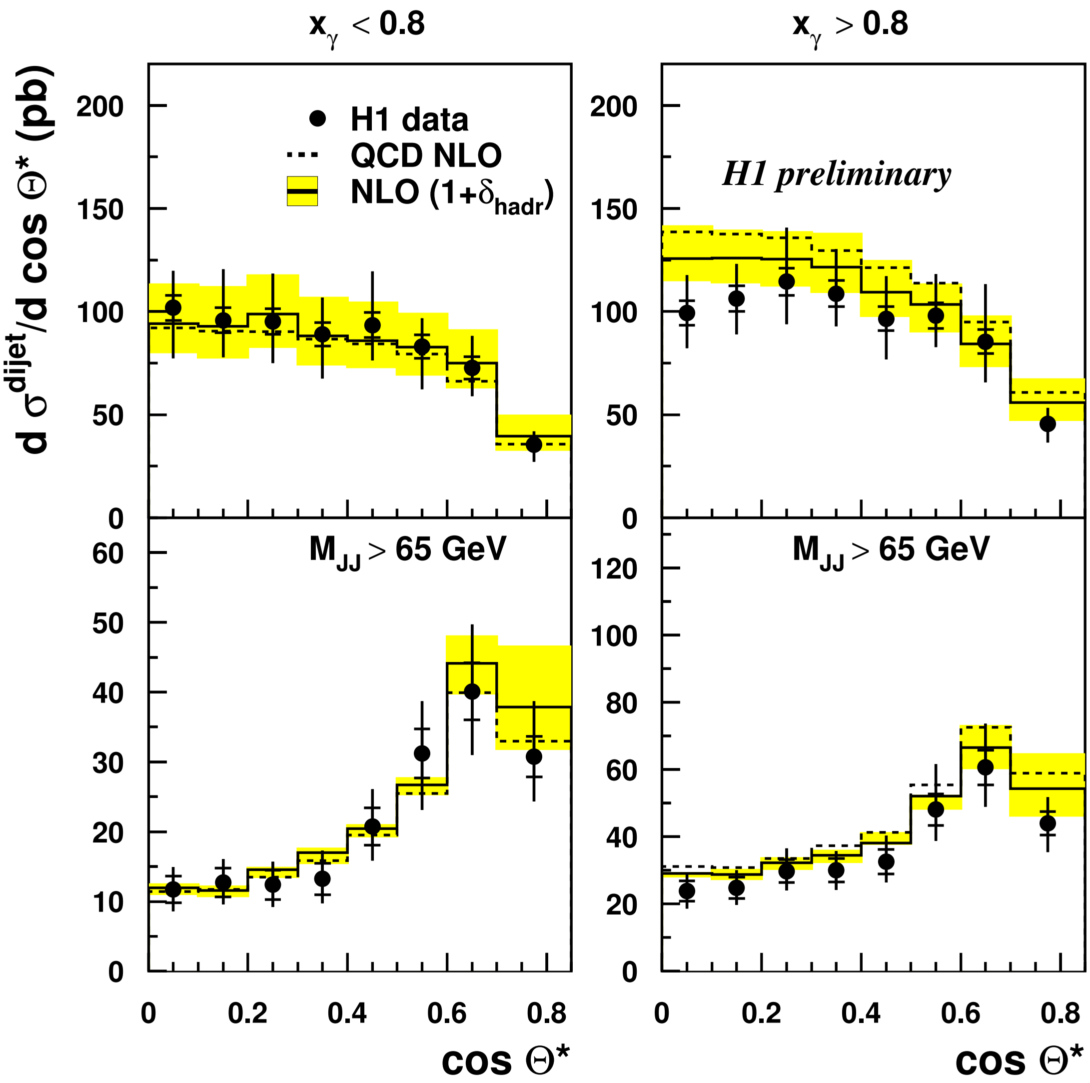

Figure 8: Differential eP cross sections for dijet production as a function of $\cos\theta^*$. The left plots shows the cross sections for the higher x_γ region, the right plots for the lower x_γ region. The lower two plots show the cross sections for an additional cut on the invariant mass of the dijet system. The inner error bars denote the statistical, the outer error bars the quadratic sum of all statistical and systematic errors of the data. The NLO predictions using CTEQ5M structure functions for the proton and GRV-HO structure functions for the photon are shown as a dashed line. NLO predictions with hadronization corrections are shown as a full line, the grey band indicates the renormalization and factorization scale uncertainties of the NLO prediction.